ECOLOGY

Hot spring oases in the periglacial desert as the Last Glacial Maximum refugia for temperate trees in Central Europe

Jan Hošek[1,2]*, Petr Pokorný[2], David Storch[2,3]*, Jiří Kvaček[4], Jeff Havig[5,6], Jan Novák[7], Petra Hájková[8,9], Eva Jamrichová[9], Latisha Brengman[10], Tomáš Radoměřský[1,11], Marek Křížek[12], Tomáš Magna[1], Vladislav Rapprich[1], František Laufek[1], Trinity Hamilton[5], Andreas Pack[13], Tommaso Di Rocco[13], Ivan Horáček[14]

Northern glacial refugia are a hotly debated concept. The idea that many temperate organisms survived the Last Glacial Maximum (LGM; ~26.5 to 19 thousand years) in several sites across central and northern Europe stems from phylogeographic analyses, yet direct fossil evidence has thus far been missing. Here, we present the first unequivocal proof that thermophilous trees such as oak (*Quercus*), linden (*Tilia*), and common ash (*Fraxinus excelsior*) survived the LGM in Central Europe. The persistence of the refugium was promoted by a steady influx of hydrothermal waters that locally maintained a humid and warm microclimate. We reconstructed the geological and palaeohydrological factors responsible for the emergence of hot springs during the LGM and argue that refugia of this type, allowing the long-term survival and rapid post-LGM dispersal of temperate elements, were not exceptional in the European periglacial zone.

INTRODUCTION

A classical paradigm of European historical biogeography states that interglacial elements survived the harsh conditions of the most extreme glacial stages in refugia situated in the Mediterranean peninsulas of Europe and, then, after the climatic amelioration, spread to the north and recolonized most of the continent (*1*–*3*). Over the past three decades, studies based on molecular phylogeography (*4*–*7*), pollen evidence (*8*), and ancient DNA (*9*) indicated that some temperate taxa might also have survived the harsh glacial conditions in isolated cryptic northern refugia (*10*, *11*) situated north of the eastern Alps (above ~45°N). With an increasing number of case studies (*12*, *13*), meta-analyses (*9*, *14*, *15*), theoretical considerations (*16*, *17*), and models (*18*–*20*), the idea of cryptic northern refugia has become a hotly debated hypothesis to explain the genetic diversity of many West Palearctic temperate clades [including temperate trees; (*17*, *21*–*23*)], as well as the unexpectedly rapid rate of their re-expansion following late Pleistocene climatic amelioration.

Nevertheless, a critical reexamination of this topic (*24*) demonstrated that actual support for the predicted refugia is rather weak and that direct evidence of the continuous survival of temperate taxa north of the Alps during the most critical interval of the Last Glacial Maximum (LGM) is actually missing (Fig. 1). One reason for this is the lack of a relevant fossil record from the LGM because the LGM is usually recorded in sedimentary series as a large-scale erosional event rather than an accumulation of fossiliferous deposits (*25*, *26*). Skepticism about this hypothesis stems primarily from serious doubts about the environmental factors that would be capable of supporting the persistence of temperate biota in central Europe under the cold and dry conditions of the LGM (*24*).

Here, we provide robust fossil evidence of the persistence of temperate tree taxa in the periglacial zone of central Europe during the LGM, together with geological evidence that sheds light on the driving forces which ensured the maintenance of these refugia throughout this climatically harsh period.

RESULTS

The area and the sedimentary setting

The investigated area (centered at 48°52′N, 17°7′E, 170 to 230 m above sea level) lies in southern Moravia (Czech Republic), on the northernmost part of the Vienna Basin (VB; Fig. 1). VB is a prominent sedimentary structure at the junction of the Alps, the Carpathians, and the Bohemian Massif, filled by several hundreds to several thousands of meters of Neogene marine strata (clay, sand, and clayed gravel). The area in focus exhibits a peculiar surface topography, marked by distinct geomorphological features: dozens of shallow circular-to-semioval-shaped depressions (Fig. 1 and fig. S1) filled by late Pleistocene aeolian and colluvial sand (Fig. 2, B, C, and E, and fig. S1). In the area of ~50 km^2, altogether 178 circular depression structures were mapped (*27*). The diameter of the depressions varies from 38 to 324 m. Their spatial distribution is rather random, although, in some cases, it is possible to observe an arrangement in

[1]Czech Geological Survey, Klárov 3, Prague 1, Czech Republic. [2]Center for Theoretical Study, Charles University and the Czech Academy of Sciences, Jilská 1, Prague 1, Czech Republic. [3]Department of Ecology, Faculty of Science, Charles University, Viničná 7, Prague 2, Czech Republic. [4]Department of Palaeontology, National Museum Prague, Václavské nám. 68, Prague, Czech Republic. [5]Department of Plant and Microbial Biology, University of Minnesota, Saint Paul, MN 55108, USA. [6]Department of Earth and Environmental Sciences, University of Minnesota, Minneapolis, MN 55455, USA. [7]Department of Botany, Faculty of Science, Charles University, Benátská 2, Prague 2, Czech Republic. [8]Department of Botany and Zoology, Faculty of Science, Masaryk University, Kotlářská 2, Brno, Czech Republic. [9]Department of Paleoecology, Institute of Botany, The Czech Academy of Sciences, Lidická 25/27, Brno, Czech Republic. [10]Earth and Environmental Sciences Department, University of Minnesota Duluth, Duluth, MN 55812, USA. [11]Institute of Geology and Palaeontology, Faculty of Science, Charles University, Albertov 6, 128 43 Prague 2, Czech Republic. [12]Department of Physical Geography and Geoecology, Faculty of Science, Charles University, Albertov 6, Prague 2, Czech Republic. [13]Universität Göttingen, Geowissenschaftliches Zentrum, Goldschmidtstraße 1, Göttingen, Germany. [14]Department of Zoology, Faculty of Science, Charles University, Viničná 7, Prague 2, Czech Republic.
*Corresponding author. Email: jan.hosek@geology.cz (J.H.); storch@cts.cuni.cz (D.S.)

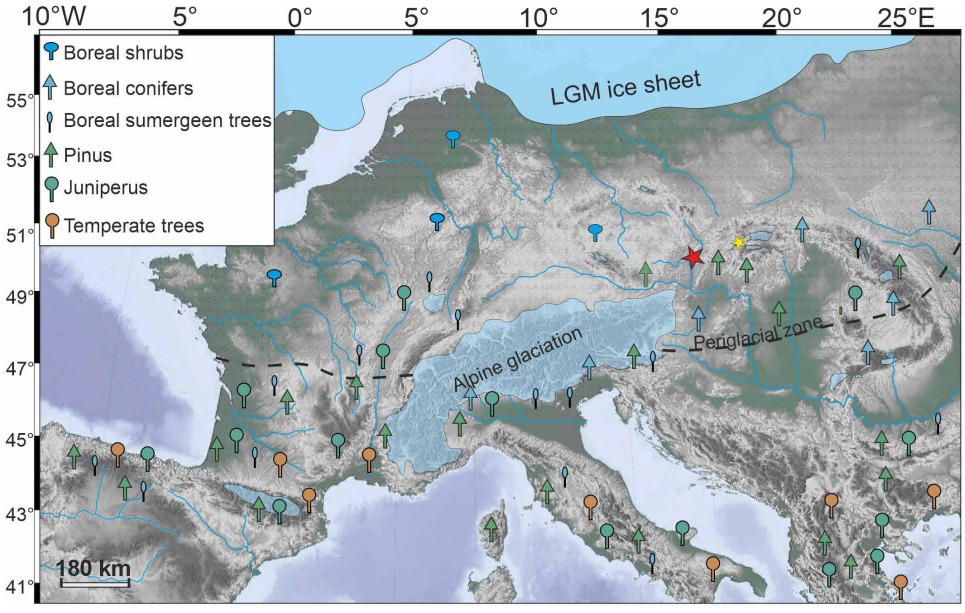

Fig. 1. European paleoenvironments during the LPG (~28 to 14.7 ka). The location of the newly recovered deposits in Moravia (red star) and a hydrothermal field in the Liptov Basin (yellow star), along with the distribution of previously investigated sites with macrofossil tree findings dated to the Late Pleniglacial [LPG; modified from (*24*)]. The maximum extent of glaciers [blue; after (*106*)] and the southern limit of the permafrost (periglacial) zone [dashed line; after (*79*)] are also depicted.

lines in the southwest-southeast direction, concordant with fault structures and the current drainage system of the area.

Twenty-one selected structures were investigated in detail either by boreholes, electrical resistivity tomography (ERT), or excavated trenches (table S1; see Materials and Methods). The lithological record of the investigated structures consists invariantly of (i) 1- to 5-m-thick aeolian and colluvial sand and fossil soil horizons dated to the late Pleistocene (*28*), which overlay (ii) quasi-continuous horizons of the thinly laminated, silica-rich sedimentary unit up to 40-cm thick (Fig. 2E and fig. S2), containing diverse plant macroremains. The horizon of silica-rich sediment is separated from the bedrock Miocene sediments (clayed sand to clayed gravel) by a thin layer of colluvial sediments or lies directly on the eroded bedrock surface (fig. S2 and supplementary text A).

Petrographic and geochemical investigations of the silica-rich sedimentary unit reveal evidence of authigenic silica precipitation and silicification in a terrestrial setting (supplementary text A and C, table S2, and figs. S4 to S8). We therefore interpret these deposits as silica sinters—remnants of ancient hot springs that were formed when warm, near-neutral pH water, oversaturated with respect to silica, cooled down, and evaporated at the surface (*29*, *30*). Results of the triple-oxygen-isotope–based temperature model (fig. S17 and supplementary text B) give water temperature estimates of ~15° to 35°C.

The occurrence of silica sinters yields a unique phenomenon, so far unreported in the European Quaternary past. Direct field and laboratory-based comparisons (supplementary text C and figs. S19 to S26) indicate that Moravian fossil sinters are almost identical to those produced by extant hot spring systems in North America (Fig. 3). These sinters formed in low-temperature (<40°C) environments in shallow thermal pools, in their outlet channels, and, according to revealed textures (supplementary texts A and C), mostly in geothermally influenced marsh areas surrounding individual pools (Fig. 3).

Chronological framework of hot spring discharge

The studied silica sinters are rich in numerous organic macro- and micro-remains, including stems, branches, mosses, seeds, leaves, pollen, and microbes. The preservation of abundant plant remains in authigenic silica sinters allowed the radiometric dating using radiocarbon (^{14}C) measurements (*31*–*34*). Thirty-two radiocarbon ages of organic carbon extracted from 28 samples (table S3, Fig. 4, and fig. S9) range from 11.168 calibrated years before the present (cal yr B.P.; Early Holocene) to 34.768 cal yr B.P. [i.e., Weichselian Middle Pleniglacial (MPG), corresponding to the marine isotopic stage (MIS) 3], with most ages ($n = 25$) referring to the Weichselian Late Pleniglacial [LPG; MIS 2; 28 to 14.7 thousand years (ka)].

Radiocarbon dating of both bulk sediment and the uppermost layer of silica sinters with preserved leaves was performed on three samples, and all obtained ages were found to be in stratigraphical order (table S3 and fig. S10). In two cases, median ages show only negligible differences of 102 and 548 years, whereas, in a single sample, a much larger difference of about 8 ka was measured (table S3 and fig. S10). In addition, two measurements of the bulk material from one sample were conducted, and the data obtained show a difference in calendar ages of about 150 years (fig. S10).

Radiocarbon data show that hydrothermal water discharge occurred across the time intervals of 11.2 to 34.3 ka at site HoDo1, 13.4 to 30.7 ka at site HoDo2, and 22.9 to 34.8 ka at site HoDo 4. At site HoDo3, the single acquired date indicates hydrothermal activity at ~22.9 ka (fig. S9).

The lithostratigraphic record does not allow an assessment of whether the hydrothermal discharge was continuous or limited to the intervals for which the ^{14}C data are available. However, considering that, out of the total area of the studied hydrothermal field, only a few depressions have been investigated (Fig. 1 and fig. S1), it seems very likely that additional hydrothermal water discharge occurred at sites that have not yet been excavated and dated. The

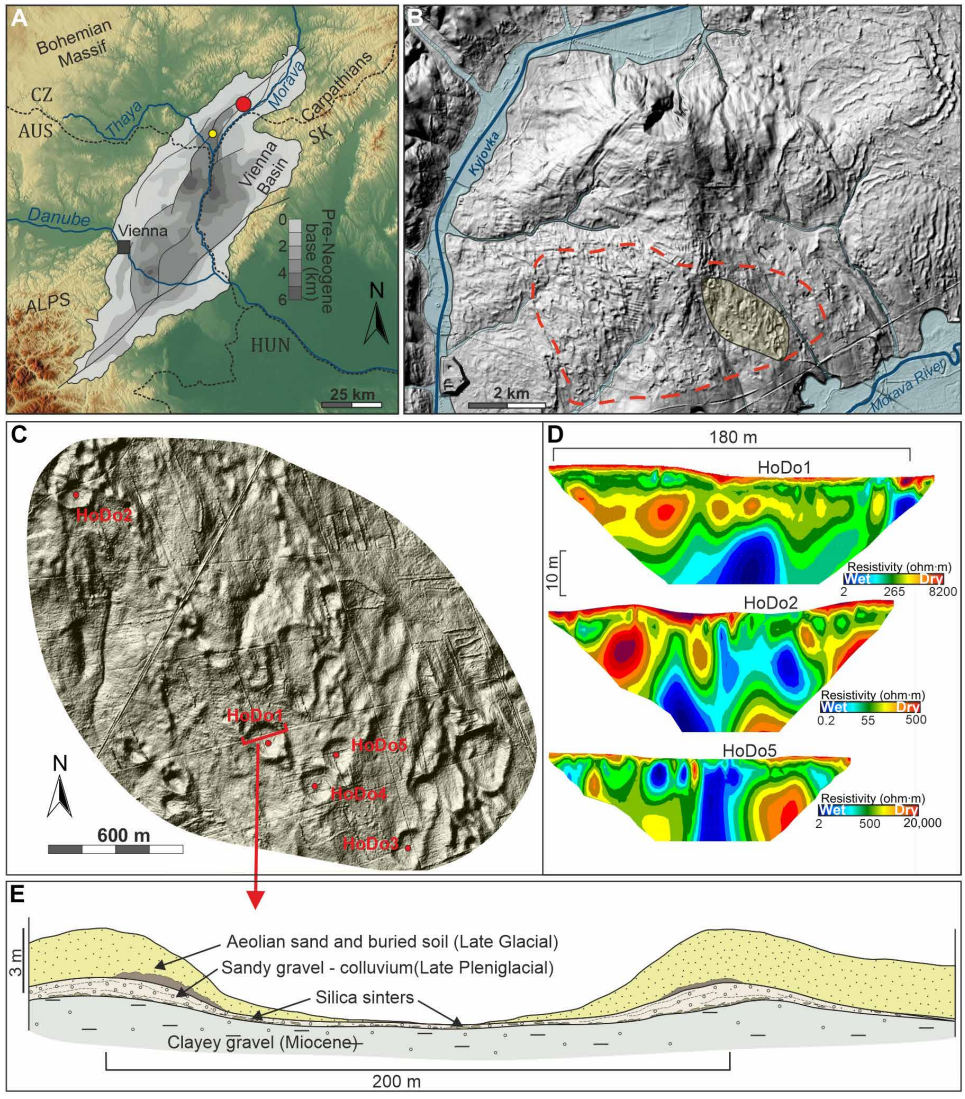

Fig. 2. Regional and local geomorphological and geological settings of the Moravian fossil hydrothermal field. (**A**) The tectonic overview and bathymetry of the VB [modified from (*74*, *107*)] and the locations of the studied Moravian hydrothermal field [red circle, detailed in (B)] and nearby peat deposits (yellow circle; see Supplementary Materials). (**B**) Digital Terrain Model showing tens of distinct shallow circular-to-semioval-shaped depressions covering an area of about 50 km^2 (red dashed line). (**C**) A close-up view of the surface topography [yellow colored polygon in (B)] with the marked depressions that were studied in detail. (**D**) Results of the electrical resistivity tomography (ERT) of three investigated depressions. Distinct low-resistant vertical structures (blue color) point to wet/mineralized zones and suggest the location of the depressions on a fault. (**E**) Cross section of one of the studied depressions shows a quasi-continuous horizon of silica sinter deposits overlaid by Late Glacial colluvial sediments and aeolian sands.

between-site differences in dating can be ascribed to episodic alternation in discharge intensity and silica sinter formation among neighboring aquifers. Such an assumption is consistent with temporal and spatial dynamics observed in modern hydrothermal environments worldwide (*35*–*37*), showing that hot spring discharge may be highly episodic with alternating phases of silica sinter formation and destruction and the timescale between discharges can range from centennial to millennial (*35*). This implies that, in particular sites, the hot spring discharge and associated silica sinter deposition may have occurred irregularly, interrupted by erosional processes and time gaps between deposition. Such circumstances could explain distinct lithological unconformities found in some samples (supplementary text B and fig. S3) and the fact that, in a single case (sample KS3_C2), the radiocarbon age of the uppermost layer was about 8 ka younger than the age obtained from the bulk (fig. S10). In summary, the studied area was a basin with high spatiotemporal dynamics of hydrothermal discharge whose activity was restricted to the terminal stages of the last glaciation.

Floral record from the silica sinters

Pollen record

Pollen analysis was undertaken for 25 sinter samples. Although results suffered from poor pollen preservation, five samples provided well-preserved pollen spectra that suggest a rich community dominated and co-dominated by temperate tree taxa (Fig. 4B and table S5); their arboreal pollen component contains a large number

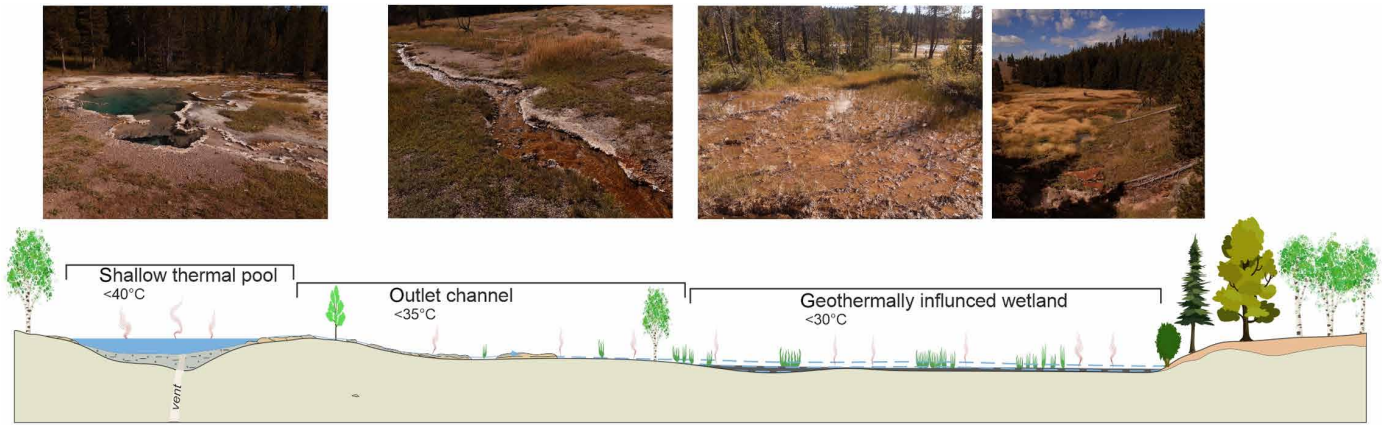

Fig. 3. Interpreting the depositional environment of the past hydrothermal field in Moravia. Idealized cross section through the depression hosting the thermal spring, as evident from field and laboratory-based comparisons with modern systems (figs. S19 to S26 and supplementary text C). The thermal water-fed pool is surrounded by a low silica sinter rim, through which the outlet streams flow. The outlet channels provide a habitat for sparse vascular plant vegetation on interfluve. The outlet channels feed the distal wetland with diverse vegetation. Photographs above the sketch show respective habitats as mapped in active hot spring areas of Yellowstone National Park (supplementary text C and fig. S19; research conducted under Yellowstone Research Permit YELL-2022-SCI-7020).

of deciduous trees (*Alnus glutinosa* t., *Corylus avellana*, *Quercus*, *Sorbus* t., *Tilia*, and *Ulmus*) and spruce (*Picea*). Because of their dominance in pollen spectra, we consider this finding to be proof of local occurrence in the vicinity of thermal springs. This contrasts with the background pollen signal that includes the dwarf birch (*Betula nana*) and herbaceous taxa characteristic of periglacial open landscapes—Chenopodiaceae, *Dryas octopetala*, *Helianthemum*, and *Artemisia* (table S5), i.e., elements of cold steppe and tundra. We consider this contrast to be a strong line of evidence of environmental contrast between local, micro-climatically improved conditions and a significantly harsher periglacial landscape in the wider area. It is impossible to estimate the spatial arrangement of these ecologically contrasting (temperate versus boreo-continental) habitats only on the basis of pollen analysis, but, because the periglacial steppe-tundra was the prevailing biome of the entire region (*7*), it is reasonable to assume that the forested environment represented an island or "archipelago" of habitats suitable for the temperate organisms within the matrix of the harsh periglacial landscape.

Plant macroremains

Our record is extraordinarily rich in macrofossils of arboreal taxa. The most common finds are the branches and needles of Scots pine (*Pinus sylvestris*) and branches of spruce/larch (*Picea*/*Larix*). Macrofossils of broad-leaf tree taxa were also present in relatively large numbers.

Leaves. Fragments of leaves have been observed in many specimens, but the visualization is problematic due to overlap and the fragmented nature of the leaves preserved. Only nine samples (Figs. 5 and 6 and figs. S11 to S13) preserved patterns sufficient for robust taxonomic identification. These were radiocarbon-dated to ~26.13, 26.10, 22.65, 20.21, 19.13, 18.94, 18.50, 17.19, and 15.83 ka (Figs. 4 to 6, figs. S11 and S12, and table S3). The preserved leaf fragments are badly damaged and poorly preserved but enough remained to allow us to identify diagnostic characters in the material. These samples include fragments of central and marginal parts of leaves, with shallow lobate margins and a vein ending in the lobe tips.

A particularly well-preserved basal part of the leaf with margin, secondary veins, and one intercalary vein was found in the top layer in the sample KS3C_2 (~18.9 ka; Fig. 5A). The record from this specimen clearly indicates the undulate margin, particularly the sinus that area is irrigated by an intercalary vein. Fragments of one larger and one smaller leaf, 53- and 33-mm long, were preserved in sample KS3C_1 (~17.2 ka; Fig. 5B). Both fragments show a central vein. The larger has six incomplete pairs of secondary veins, and the smaller has only fragments of secondaries but includes a basal margin. Two marginal lobes and a central vein have also been observed in this sample (Fig. 5C). Primary and secondary venation and a higher-order venation pattern have been identified in several other samples (figs. S11 and S12). In all cases, the venation is alternately pinnate with one or several intercalary veins.

Observed venation patterns (pinnately craspedodromous with intersecondaries/intercalaries) cannot be associated with any European cold-tolerant deciduous trees [*Betula*, *Populus*, *Frangula*, and *Salix*; (*38*)] nor with most temperate tree species (e.g., *Acer*, *Alnus*, *Ulmus*, *Fagus*, and *Sorbus*; see the detailed comparison in Table 1). As the craspedodromous venation with intercalary veins in combination with the lobate margins is the characteristic taxonomic sign for leaves of *Quercus*, we conclude that all the examined leaf fragments represent most likely leaves of oak (*Quercus*). Such an assumption is further supported by the wood anatomy investigations (see below). The presence of only one foliage type in the record can be explained by the fact that oak leaves have a much greater preservation potential compared to leaves of other deciduous trees (*39*).

There are 531 oak species described worldwide (*40*). However, in Northern and Central Europe only two, namely, *Quercus petraea* and *Quercus robur*, occur in cold temperate forests (*41*). The two species differ not only in a number of traits, particularly in their leaf shape, acorns, and cupulas [e.g., (*42*–*44*)] but also in their leaf venation pattern (Table 1). The intercalary veins are frequently present in the leaves of *Q. robur*, while they are absent in the leaves of *Q. petraea* (*45*). Therefore, intercalary veins found in the studied fragments indicate that the fragments that come from leaves of *Q. robur* grow preferentially in wet conditions, so its autecology fits well with the reconstructed paleoenvironment of the studied site.

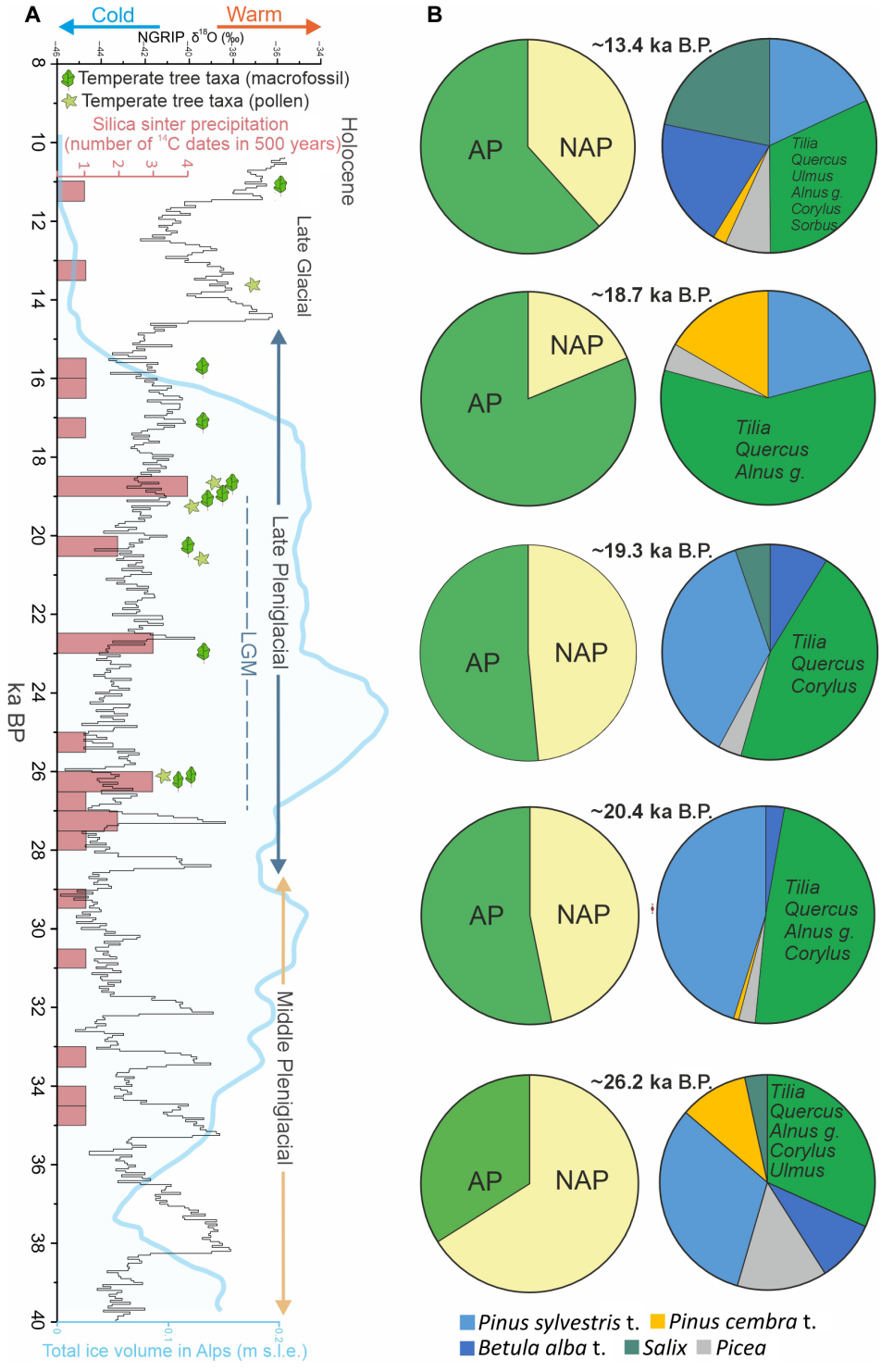

Fig. 4. Stratigraphy and fossil plant records from the late Pleistocene silica sinters. (**A**) Frequency distribution of radiocarbon data of organic matter separated from the silica sinter, correlated with the climatostratigraphic record of the time interval of 40 to 10 ka [black curve; the $\delta^{18}O$ values of NGRIP; (*35*)] and the modeled total ice volume of the glacier in the Alps (*82*) expressed in meters of sea level equivalent (m s.l.e.; blue curve). (**B**) Pollen record from the silica sinter showing the proportion of arboreal (AP) and non-arboreal (NAP) pollen components (left column) and the proportion of broad-leaved temperate taxa in the overall AP spectra (right column).

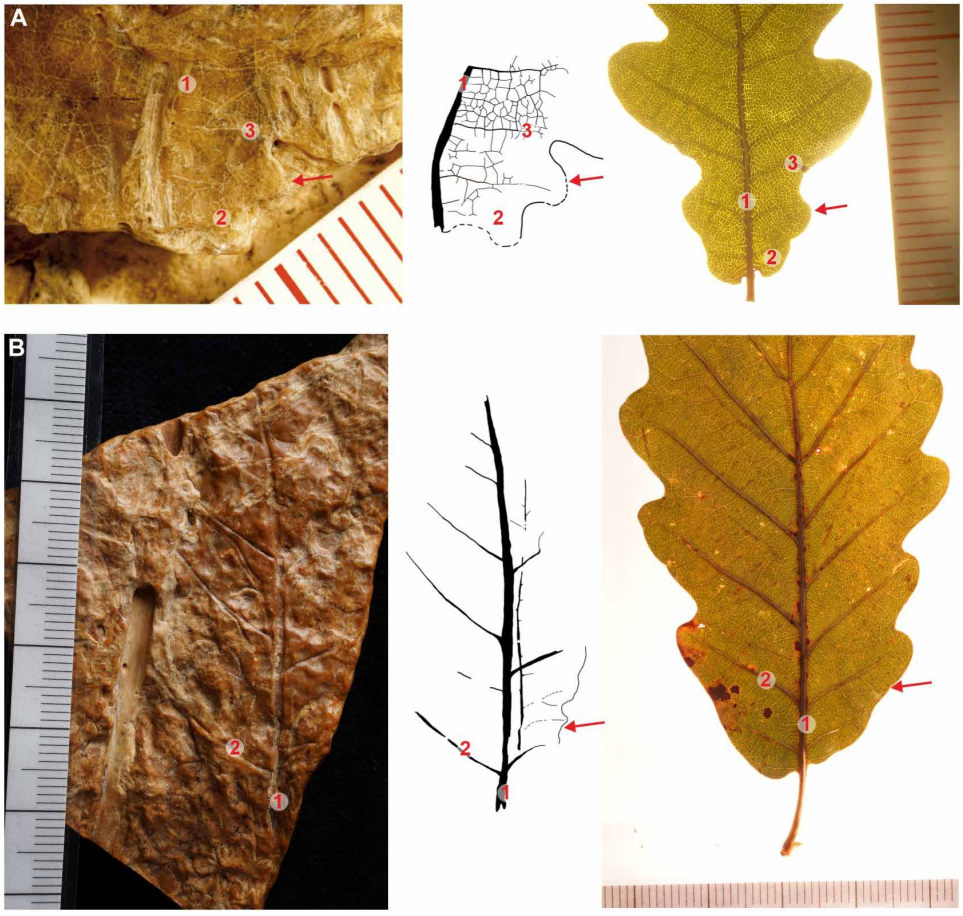

Fig. 5. Fragments of leaves preserved in silica sinter compared to recent leaves of common oak (*Q. robur*). (**A**) Basal part of small leaf with preserved main midrib (1), basal part of lamina (2), margin (arrow), and venation showing the position of intercalary vein (3) running to the lobe sinus (specimen KS3C_2). (**B**) Specimen KS3C_1 showing two leaf fragments with main midrib (1) and secondary veins (2); the larger leaf shows secondary veins leaving the primary vein in sharp angles, and the smaller leaf fragment shows basal part of lamina with partly preserved margin (arrow); for high-resolution images, see fig. S13.

Wood record. Overall, our wood record is dominated by conifers, of which *Pinus* branches are the most abundant, with *Larix*/*Picea* wood occurring less frequently (fig. S14). The presence of wood fragments belonging to deciduous trees is also documented in many samples, but their taxonomical interpretation is usually more problematic, due to missing anatomical traits.

Scanning electron microscopy (SEM) imaging of the twig fragment preserved in the surface layer of the sample KS3C_1 (~17.2 ka) revealed well-preserved rounded tracheas, about 50 μm in diameter (Fig. 7C). This is a typical diagnostic sign of oak wood and/or elm, not associated with the wood structure of any other deciduous tree (*46*). Given the leaf record on the same specimen (Fig. 5), it seems more likely that the twig belongs to an oak. This is further supported by the presence of a leaf bud on the twig, which is barrel-shaped, composed of several scales (Fig. 7B) and generally corresponds well to that of oak. Isolated tracheae of the same size and shape were further observed in sample KS3_X1 (~26.1 ka; fig. S14A).

Specimen KS9_fraxinus (~11.2 ka) comprises a twig with a well-preserved conical and sedentary bud sitting above the leaf scar (Fig. 7A). The bud was identified to belong to common ash (*Fraxinus excelsior*).

Conspicuous spiral thickenings of longitudinal tracheid, generally homogeneous rays, occasionally also with a row of square marginal cells of longitudinal tracheid documented in the undated sample HoDoWht (fig. S13B) indicate the presence of lime (*Tilia* sp.).

Other plant macro-remains. Ovoid female reproductive structures, including seeds preserved in situ, were recorded in samples KS3C_2 and KS3_X1 (fig. S14). The cast of the reproductive structure (fig. S15, A and B) consisting of spirally arranged scales is of particular importance. A partly distorted reproductive structure shows a well-preserved scale and several spherical seeds 2 mm in diameter (fig. S15C). The shape and size of the structure, scales, and seeds are identical to those of *A. glutinosa*.

Ovoid 4.0- to 6-mm-long and 1.3- to 2.1-mm-wide seeds found in 12 samples (fig. S16A) correspond clearly to those of *Najas marina*, a submersed plant inhabiting shallow alkaline or pH neutral water with a temperature range of 15° to 30°C in high vegetation season (*47*). The frequent occurrence of *N. marina* in the record is

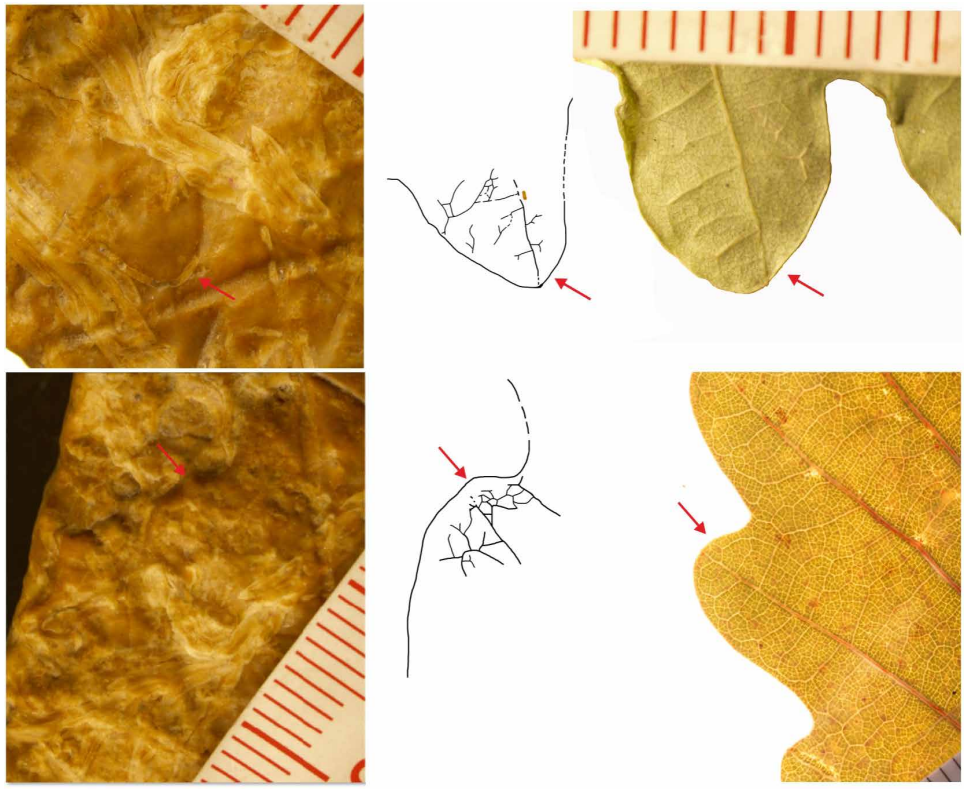

Fig. 6. Two fragments of lobes showing veins running to apex (arrow), typical character of craspedodromous type of venation.

Table 1. Identification key of European woody dicots. The key is based on leaf venation (**A**) and margin (**B**) patterns.

A	**1**	a) Venation pinnate	**2**
		b) Venation basal actinodromous	*Acer* and *P. alba*
		c) Venation imperfect actinodromous	*Tilia* and *Populus*
	2	a) Venation craspedodromous	**3**
		b) Venation brochidodromous,eu-camptodromous	*Salix* and *Frangula*
		c) Venation semicraspedodromous	*Fraxinus*, *Rosa* (some species), and *Sambucus*
	3	a) Intersecondaries present	**4**
		b) Intersecondaries absent	*Betula*, *Alnus*, *Carpinus*, *Fagus*, and *Rosa* (some species)
	4	a) Intersecondary one (if any)	*Rosa* (some species)
		b) Intersecondaries more than one	***Q. robur* and *Quercus pubsecens***
B		a) Margin entire	*Acer* (some species), *Fagus*, *Salix* (some species), *Hedera*, and *Frangula*
		b) Margin serrate	*Acer* (some species), *Carpinus*, *Corylus*, *Sorbus*, *Ulmus*, *Tilia*, *Fagus*, *Rosa Fraxinus*, *Salix*, *Betula* (some species), and *Alnus*
		c) Margin crenulate	*P. alba* and *P. tremula*
		c) Margin lobate	***Quercus*** (European temperate species)

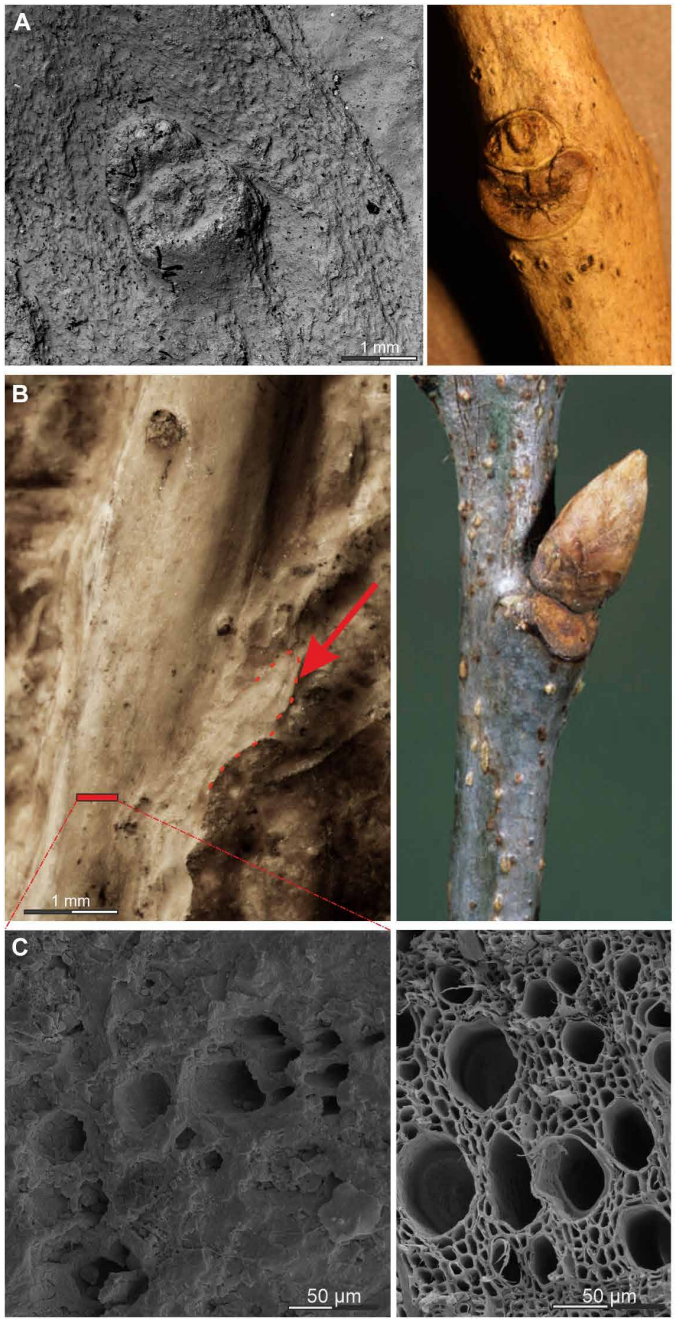

Fig. 7. Examples of wood fragments preserved in silica sinter. (**A**) Scanning electron microscopy (SEM) image of twig with bud identified as *F. excelsior* (common ash) compared to recent twig of common ash (specimen KS9_fraxinus). (**B**) The twig with a bud (arrow) identified as *Quercus* sp. compared to recent twig of common oak (specimen KS3C-1). (**C**) SEM image showing silicified vessels (transverse section) of *Quercus* sp. preserved in wood fragment from the twig in (B; red line) in comparison with recent wood of *Q. robur*.

consistent with the presumed sedimentary environment and the abovementioned stable isotope-based water temperature estimates (supplementary text B). Three-millimeter-long leaves and 0.3-mm-wide stems of nonvascular plants found in those same samples (fig. S16B) were identified as in situ–silicified remnants of moss *Bryum* cf. *schleicheri*.

LPG and Late Glacial paleobotanical records from neighboring areas

To test the idea that geothermal areas could enhance microclimate conditions during the late Pleistocene, we carried out a paleobotanic investigation of the calcareous lacustrine sediments located within the active hydrothermal field of the Liptov Basin in Western Carpathians, Slovakia (Fig. 1, fig. S28, and supplementary text D). Although no plant macrofossils were recovered from the 600-cm-long core, the local survival of temperate biota during the LPG was demonstrated by the pollen record obtained (fig. S29A). Substantial and consistent amounts of pollen of temperate tree taxa (namely, *Quercus*, *Alnus*, and *Ulmus*) revealed from sediment layers dated to the interval between 20 and 15.5 ka (table S4) strongly support the occurrence of these temperate taxa in the proximity of hot springs in the larger geographic scale.

Another investigated site is located ~30 km southwest of the ancient hydrothermal field (Fig. 2A). About 400-cm-long sedimentary core recovered from the filled-in oxbow lake covers the period of the Bölling-Alleröd interstadial (~14.7 to 12.7 ka) according to four radiocarbon data from the plant macroremanis (table S4). Revealed pollen record (fig. S29B) also shows an unexpectedly high amount (~1 to 2.3%) of pollen from temperate trees: *Quercus*, *Ulmus*, *Corylus*, *Tilia*, and *Fraxinus*. Moreover, in the layer dated to 14,533 cal yr B.P., a piece of *Quercus* wood was found and directly radiocarbon-dated to 14.56 ka (table S4).

.

DISCUSSION

Robustness of the radiocarbon data from silica sinters

Radiocarbon dating of silica sinter deposits has previously been applied to a number of active and inactive geothermal areas around the world [e.g., (*32*–*34*, *48*–*53*)]. Similar to other spring deposits such as calcareous tufa or travertine, ^{14}C dating of separated organic matter is considered the most robust approach to obtaining accurate chronology of spring discharge (*34*). However, the results of some research [e.g., (*53*, *54*)] have found radiocarbon dating to be potentially problematic, mainly due to the geobiological peculiarities of the thermal springs. To address possible doubts about the reliability of the obtained radiocarbon data, we first discuss potential limitations that may come here into account:

(i) In some studies, inconsistencies between radiocarbon ages and the stratigraphic position of samples have been attributed to the incorporation of microbial mats (namely, *Chloroflexus* and *Chloroflexus*-like organisms), which metabolize old carbon present in thermal groundwater (*52*, *53*). However, because these bacteria show $\delta^{13}C$ values ranging between −10 and −16 per mil (‰) (*55*), i.e., significantly higher values than other organic matter in the silica sinter (usually <−20‰), stable carbon isotope compositions in dated material can be used to evaluate whether the organic matter is contaminated and thus provides an unreliable age (*52*). Our samples show $\delta^{13}C$ values ranging around −29‰ (table S3), indicating that analyzed organic matter has minimum (or no) bacterial organic matter contamination. Consequently, the old carbon effect, reported from some reference sites, can be excluded for samples in our study. (ii) It has also been reported from active volcanic areas that high volumes of CO_2 emitted from the hydrothermal springs may potentially introduce old carbon to the plants growing in the vicinity of the vent. The vegetation affected by ^{14}C-free magma-derived CO_2

then provides radiocarbon ages up to 4000 years older than expected (*54*). However, as the study area is not associated with any active magmatic system, which could be the source of significant CO_2 emissions, such an effect is very unlikely in these settings. This assumption is further supported by the fact that no traces of carbonates (such as calcite or siderite) were found in studied silica sinters. If the CO_2 tension in hydrothermal water from which the deposits precipitated was enlarged, the traces of carbonates would be expected. Moreover, the assimilation of magma-derived CO_2 by plants is usually strongly correlated with enrichment of ^{13}C with values about 4 to 10 ‰ higher than the normal atmosphere (*56*, *57*). However, such isotopic enrichment was not observed in the $\delta^{13}C$ record of the organic matter from silica sinters, which shows typically low values (~−29‰) corresponding to the record of most C3 plants (*24*). (iii) Contamination of the dated organic material by ^{14}C by depleted (dead) fossil carbon from pre-Quaternary sediments/bedrocks ["old-carbon effect"; (*58*, *59*)] can also be ruled out in our case as the bedrock sediments consist of noncalcareous sand and sandy clay. Furthermore, any potential traces of fossil carbon were leached during the pretreatment by acid solutions (see Materials and Methods). (iv) Last, the chronological framework suggested by the radiocarbon dates is supported by the lithostratigraphic context: The silica sinters dated to the LPG underlay aeolian sands directly dated to the Late Glacial period (Fig. 2 and fig. S2) (*28*, *60*). For the reasons listed above, the radiocarbon-based stratigraphy of the sinters in the present study can be considered robust and accurate.

Paleoenvironmental settings

Despite the cold climatic conditions of the LGM (*61*, *62*), discharged hydrothermal water likely maintained conditions similar to some areas of the recent Arctic, where thermal springs and their surroundings remain ice- and snow-free year-round, even with a discharge water temperature of only 5°C (*63*). In periglacial environments of the LGM, such circumstances could have enhanced permafrost degradation, resulting in surface subsidence and the formation of distinct waterlogged depressions, consistent with those mapped in the study area (Fig. 2B and fig. S1).

On the basis of these findings, we can infer that, during the LGM, most of the mapped terrain depressions hosted thermal springs with a wetland environment in their surroundings. Such mesic or even hydric habitats would have radically differed from the presumed LGM environment characterized by critically low precipitation (*64*), in which a lack of liquid water was the most limiting factor for biota (*18*). The evaporation of warm water and its penetration into the surrounding substrate would have increased local humidity and soil moisture, providing optimal microclimatic conditions that supported temperate biota development within the periglacial desert. A recent analogy can be seen in geothermal/hydrothermal regions in cold and arid landscapes of tundra and polar deserts (*65*), where warmer soil and stable hydroclimatic conditions create thermal oases supporting enhanced biological production, diversity and extrazonal occurrence of biological taxa (*66*–*68*).

Paleobiogeographic relationships

The paleobotanical data presented here constitute the first direct evidence of an LGM temperate ecosystem north of the Alps. This has far-reaching biogeographic and paleogeographic implications. It opens the possibility that temperate forest species were able to survive in some parts of central Europe continuously for the past tens of thousands of years, including the LGM. The regional pollen (*69*) as well as charcoal records from archeological sites and soils (*70*–*72*) show that temperate trees including *Quercus*, *Tilia*, *Fraxinus*, *Alnus*, *Ulmus*, *Sorbus*, and *Corylus* grew in Moravia during the second part of the MPG (~45 to 28 ka; Fig. 4), with the most diverse woody assemblages dated to the interval between 35 and 30 ka (*7*). Until now, the consensus has been that these taxa were not able to survive in these latitudes under the cold and dry climates of the subsequent harsh period of the LPG. The present record demonstrates their continuous survival in the studied region throughout the whole LGM period. The putative role of the Moravian refugium as a source of the early spread of temperate plant taxa in the post-LGM stage is further supported by the paleobotanical record revealed from peat deposits located 30 km from the study area (Lanžhot site; Fig. 2A and supplementary text D). Both the high proportion of pollen of thermophilous tree taxa in the pollen record (fig. S29B) dated to the Late Glacial (14.7 to 12.7 ka; table S4) and especially the preserved 14.56-ka oak wood suggest that temperate species migrated from the Moravian geothermal refugium almost simultaneously with the first climate amelioration after the LPG.

Sources and maintenance of refugial conditions

Hot spring discharge restricted to the Weichselian LPG represents another fascinating aspect of our discovery. To explain this phenomenon, the following regional geological and hydrogeological features are to be recalled:

1. The studied area is situated in the NE margin of the VB, the Neogene intermountain, thin-skinned, pull-apart sedimentary complex bordering the Alps, the western Carpathians, and the Bohemian Massif (Figs. 2 and 8A). The pre-Neogene bedrock of the porous permeable sediments forms a gradual slope from shallow basin margins into a more than 5000-m-deep depression in its northern part (*73*, *74*). This structure is disposed to canalize surface and subsurface water masses from neighboring slopes of the Alps, the Carpathians, and the Bohemian Massif (Fig. 8A). The tectonic faults penetrating the pre-Neogene bedrock interconnect the hydrological system of the VB with geothermal deep-circulation systems (*75*). The increase in surface hydrothermal influx, dated to the time interval between 35 and 11.4 ka, was synchronous with the period of highest hydro-climatic fluctuations during the last climatic cycle (Fig. 4) (*76*).

2. The relations between hydrothermal activity, geological setting, and supra-regional climate could then be particularly attributed to the following factors: (i) During the late MPG (MIS 3) with a relatively humid climate (*77*, *78*) and a limited extent of permafrost (Fig. 8B) (*79*), the lowland area of the VB was saturated by surface and subsurface water flowing from the neighboring Bohemian Massif highlands (*27*) and the repeated large-scale melting of the Alpine glaciation (*80*). In consequence, the porous infill of the deep center of the VB has been oversaturated by percolating deep water. A prolonged percolation of large water masses in the deepest parts of the VB situated close to the study area resulted in gradual enrichment of these waters with silica. (ii) The initiation of the Moravian hot spring refugium at the end of MPG (MIS 3) and during LPG (MIS 2) was probably stimulated by regional tectonic activity (*81*) that increased due to the cyclic growth and disintegration of the glaciation during the LGM in the eastern Alps (southwest margin of the VB). (iii) The abruptly growing Alpine glacial complex (Fig. 4) extended, in that period, to the lowlands in the southern part of the VB (Fig. 8C) (*82*).

Large amounts of water produced by its melting at lower elevations during the LGM interstadials and summer seasons (*80*) canalized into the bottom of the VB, recharged the deep roots of the geothermal aquifers, and, at the same time, exerted hydraulic pressure that raised deep hydrothermal water to surface circulation (Fig. 8C). With the decline of such glaci-hydrological forcing following the end of the last glacial period, the surface geothermal aquifers in the region calmed down and disappeared.

Notwithstanding the unique settings of the study site, hydrothermal discharging is relatively common in eastern central Europe (*81*), suggesting that there might have been many additional sites that provided comparable microclimatic conditions during the LGM. This holds especially for the Pannonian Basin and Carpathian Mountains foreland—a region of hundreds of Pleistocene to Holocene calcareous hot springs (*81*) and a possible location for an extra-Mediterranean macro-refugium according to phylogeographic (*10*, *83*) and both paleobiological and biogeographical evidence (*84*–*89*). Such an assumption is strongly supported by the pollen record obtained from the Liptov Basin in Slovakia (supplementary text C and fig. S29A). Despite a lack of data from the peak stage of LGM, this finding, in turn, supports the idea of a considerable role played by hydrothermal sites in enabling the persistence of temperate organisms in central Europe. Such hydrothermal areas might have provided stable conditions for the long-term maintenance of refugia for numerous elements of temperate biota as well as humans and acted as significant "stepping stones" for the expansion of their ranges during the climatic amelioration of the Late Glacial Interstadials (14.7 to 12.7 ka) and after the Pleistocene/Holocene warming (11.7 ka). Thus, despite the rather limited dispersal capacity of many temperate taxa, the postglacial rearrangement of European biota could have proceeded rapidly (*88*).

MATERIALS AND METHODS

Survey methodology

The studied terrain depressions were mapped using a high-resolution digital elevation model [the Czech State Administration of Land Surveying and Cadaster(s) CUZK, 1-m grid]. Fieldwork was carried out between 2019 and 2022 for detailed geomorphologic mapping and sampling. The sedimentological record of depressions was investigated in 16 trenches excavated in five individual depressions (HoDo1 to HoDo5). The 1- to 3-m-deep and 2-m-wide trenches followed the transects going through the edges of the depressions toward their centers. Sedimentological descriptions and photographic documentation were done for each trench, and silica sinters were collected for laboratory analyses at approximately even spacings <1 m. Approximately 200 samples of siliceous sinters from five sites (0.2 to 2 kg of sample) were collected, and 106 samples were subsequently analyzed by a series of analytical techniques. A list of investigated sites is provided in table S1. Complete field data concerning individual sections and sampled material are deposited in repositories of the Czech Geological Survey and National Museum, Prague.

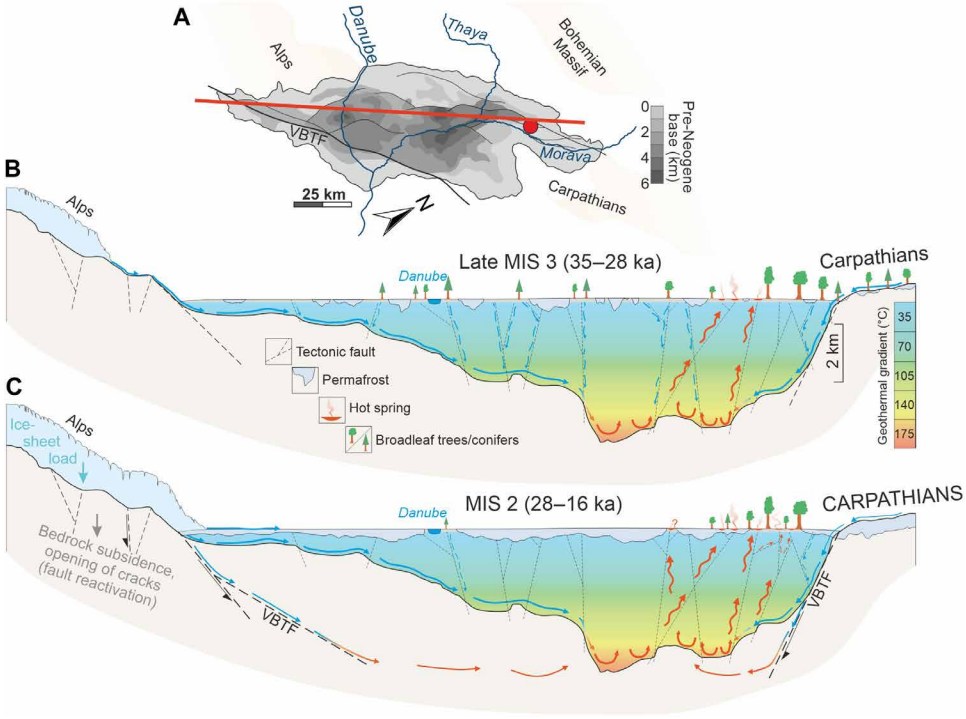

Fig. 8. Geological and hydroclimatic settings of the LGM refugium in the VB. (**A**) Bathymetry of the impermeable pre-Neogene basis of the VB [after (*74*, *106*)] with the major tectonic fault (VBTF, Vienna Basin Transform Fault) (*75*), and the location of the Moravian refugium (red circle). (**B** and **C**) Longitudinal cross sections of the VB along the red line in (A), indicating the geothermal gradients [after (*108*)], faulting (*74*, *107*), the assumed thickness of permafrost and the Alpine glacier (*82*, *109*), and respective paleobotanical records. An increased inflow of surface and subsurface water during the relatively humid Middle Pleniglacial (MIS 3) (B) percolated along major fault structures and recharged geothermal deep-water circulation systems in depths over 5 km. Cyclic growth and decay of the Alpine glacier, occurring during the late Middle Pleniglacial and especially during the LPG (MIS 2) (**C**), reactivated main tectonic structures along which hydrothermal fluids emerged as hot springs.

Ten depressions were investigated for subsurface geology using ERT. Two cross sections throughout each depression were done to acquire 12 profiles 60- to 220-m long in total. ERT acquisition was performed using an ARES II resistivity meter (AGICO s.ro. Instruments), which was connected to a linear array of electrodes evenly spaced every 2 m. Res2Dinv software (version 3.59.119, Geotomo Software) was used to convert the apparent electrical resistivity values into a two-dimensional model of the subsurface.

To compare the studied fossil sinter with modern (Holocene) records, a 2-week field campaign was conducted in 2022 within the active hot spring areas of the Yellowstone National Park (Wyoming, USA) and Borax Lake region (southwestern Oregon, USA). Samples of sinter fabrics were collected along the temperature gradient from high temperature vent with mound or hot spring pool, through mid-temperature discharge apron with a channel, to low-temperature distal areas with geothermally influenced marsh and water-logged soils (see supplementary text C for details). The sampling was specifically focused on plant-rich microfacies.

Radiocarbon dating

Twenty-eight macroscopically organic-rich sinters were analyzed for accelerated mass spectrometry (AMS) dating providing altogether 32 ^{14}C dates (table S2). Samples were collected from four individual sites (depressions), following the transects from the edges of the depressions toward their centers to obtain a representative sample of the past extent of the field, with relative stratigraphic controls. Subsampling was focused primarily on the part with macroscopically visible remains of vegetation. From the nine samples with identified leaf fragments on the surface, a thin (~0.2- to 1.0-mm-thick) layer was carefully cut away to isolate leaf tissues from other organic matter in the sinter. For the other samples, 30 to 70 g of sediment with visible vegetation remains (wood fragments, grass leaves, and seeds) was subsampled. The subsamples were rinsed with ultrapure water and dried at 60°C. Approximately one-half of the material was stored for AMS laboratory techniques, and the other half was used for SEM analyses.

Extracting organic carbon from silica sinter followed methods established by (*33*, *34*, *49*): The fine-grained material was treated in ~3 M HCl for 24 hours to eliminate inorganic carbonates and rinsed with ultrapure water. Next, the samples were immersed for 48 hours in 27 M hydrofluoric acid (HF) at room temperature, followed by the addition of fresh 27 M HF, and samples were then treated for another 12 hours at 100°C. The excess HF was evaporated, and samples were rinsed with Milli-Q water until a neutral pH was achieved. Samples were then centrifuged, residual liquid was decanted, and samples were dried at 105°C overnight. More than 0.5 mg of organic carbon per aliquot was recovered from all bulk samples, whereas only five from nine subsamples from the top layers were collected (fig. S9). SEM confirmed the presence of organic material containing mostly of remnants of plant tissue.

The samples were analyzed for ^{14}C at the Center for Applied Isotope Studies (CAIS) at the University of Georgia (23 samples; labeled as UGAMS) and at AMS laboratory in Debrecen, Hungary (nine samples; labeled as DeA). Samples were combusted to CO_2 and graphitized over a Fe catalyst using the hydrogen reduction method. The age calibrations are based on the IntCal20 curve (*90*) via OxCal v.4.4 (*91*). Calibrated ages are presented as median ages with a 2σ probability range expressed in calibrated years B.P. The ^{13}C/^{12}C ratios of 19 samples were measured separately at CAIS, using a stable isotope ratio mass spectrometer, and expressed as δ^{13}C with respect to Vienna Peedee Belemnite (V-PDB), with an error of less than 0.1‰.

Palaeobotanical investigations

Fossil plant macro-remains were studied using binocular microscopes Olympus SZX12 and Leica S9E, as well as SEM Tescan Mira3 GMU housed at the Czech Geological Survey, Hitachi 3400N housed at the Department of Earth and Environmental Science, University of Minnesota, and Hitachi S-3700N housed at the Department of Paleontology, National Museum, Prague. Taxonomic determination of wood remains was done using the reference collection and available identification wood anatomy keys (*92*, *93*).

Fragments of fossil leaves were line drawn in Adobe Photoshop, and their venation pattern was compared to leaf venation of modern species *Q. robur*, *Q. petraea*, *Tilia cordata*, *A. glutinosa*, *Betula pendula*, *Populus alba*, *Acer pseudoplatanus*, and *F. excelsior*.

From the sites with peat/lacustrine sedimentation (Lanžhot, Stankovany), 1-cm^3 volumes of samples were prepared for pollen analysis according to a standard method published by (*94*) and then stained with safranin and mounted into 1:1 water-glycerol mixtures for storage. Regarding the pollen analyses of silica sinter, about 5 to 20 g of samples was crushed and macerated in 27 M HF at room temperature for a minimum of 48 hours, before applying the above-described procedure. Although pollen is easy to extract from sinter, it is usually sparse or even absent in the record (*95*). Of 25 analyzed samples of silica sinter, only 5 samples provided a representative and reliable record. Pollen determination followed personal reference collections, available atlases (*96*–*98*), and the most recently published key (*99*).

Petrographic investigation

Mineral composition and silica precipitation textures from a total of 18 thin sections were identified using a Nikon SMZ1270/800N large-field stereoscope and Nikon Eclipse LV100N POL transmitted light microscope equipped with reflected light capabilities. We identified silicate mineral phases based on their respective diagnostic features in plane polarized and cross-polarized light, with reflected light used to distinguish oxide phases and organic material. To obtain morphological and textural data, sinter samples were examined using the SEM equipment described above, equipped with secondary electron, energy-dispersive x-ray spectrometry. The analyses were performed using an accelerating voltage of 5 to 20 keV, a beam intensity of 80 mA, and a working distance of 10 mm.

XRD analyses

Powder x-ray diffraction data (XRD) of silica sinters were collected using a Bruker D8 Advance diffractometer, equipped with a Lynx Eye XE detector and Soller slits (2.5°) in the primary and secondary beams. CuKα radiation was used. The samples were gently pulverized together with acetone in an agate mortar. To minimize the background, the samples were placed on a flat silicon wafer from the acetone suspension. Diffraction data were collected in the angular range of 4° to 80° of 2θ with a step of 0.015° for 1 s per step. An automatic divergence slit (10 mm) was used. A qualitative phase analysis was performed using the HighScore program (PANalytical, 2011) and the PDF-2 database (International Centre for Diffraction Data, 2020). Subsequent quantitative phase analysis was carried out with the Rietveld method using the

Topas 5 program (Bruker AXS, 2014). Crystal structures for low quartz, moganite, and mica (muscovite 2M1) were taken from the Inorganic Crystal Structure Database 2022. The fundamental parameter approach for the peak shape description for all phases present in the samples was used. Only scale factors, unit-cell parameters, and parameters describing profile (CrySize L) were refined. Correction for preferred orientation (March-Dollase) of mica [001] was applied. The content of the amorphous component (i.e., opal-A) was estimated from the total intensity under the defined crystalline and amorphous components in the powder XRD pattern (degree of crystallinity method).

Oxygen isotopes (silica precipitation temperature modeling)

The oxygen isotope compositions of 19 silica sinter samples were determined at the Geowissenschaftliches Zentrum, University of Göttingen (Germany), using the infrared laser fluorination method (*100*). Approximately 2 mg of aliquots were placed, along with San Carlos olivine reference material, into a multi-pit sample holder and loaded into a reaction chamber. The chamber was heated to about 60°C and evacuated overnight down to ~3×10^{-6} mbar.

Each sample was laser fluorinated by scanning the laser beam across the pit multiple times, successively increasing the laser energy up to 45 W. Approximately 150 mbar of BrF_5 was used as fluorinating agent. Following fluorination, O_2 gas was purified in the vacuum line by cryofocusing at liquid nitrogen temperature to remove condensable gaseous products and by passing through a NaCl trap heated to 150°C to passivate F2. The O_2 gas was collected with a 5-Å molecular sieve trap and then transferred via He gas stream (10 ml min^{-1}) through a 5-Å molecular sieve-packed gas chromatography column (3 m, 1/8 inch, 50°C) into a second 5-Å molecular sieve trap located before the inlet into the mass spectrometer. After evacuation of He from this trap, the purified O_2 was expanded at 50°C into the bellows of the MAT 253 Plus (Thermo Fisher Scientific, Bremen, Germany) isotope ratio mass spectrometer. Laser fluorination, gas transfer, and measurement routines were fully automated using LabVIEW software to avoid any user-specific effects. Further details on the analytical procedure are given elsewhere (*101*, *102*).

Measured oxygen isotope ratios are expressed in the delta notation ($\delta^{17}O$, $\delta^{18}O$) relative to Vienna Standard Mean Ocean Water (V-SMOW), using the calibration of San Carlos olivine on the V-SMOW scale (*101*, *103*–*105*). Deviations from mass-dependent fractionation line are expressed using $\Delta'^{17}O$ notation (Eq. 1), where

$$\Delta'^{17}O = 1000 \cdot \ln\left(\frac{\delta^{17}O}{1000} + 1\right) - 0.528 \cdot 1000 \cdot \ln\left(\frac{\delta^{18}O}{1000} + 1\right) \quad (1)$$

On the basis of replicate analyses of the San Carlos olivine, the analytical uncertainty in $\delta^{18}O$ and $\Delta^{17}O$ was taken to be ~±0.2‰ and ~±7 parts per million (1σ), respectively.

Trace element analysis

Concentrations of trace elements in a subset of geyserite samples were determined at the Czech Geological Survey, Prague, using an Agilent 7900x ICPMS. Conventional decomposition in a mixture of 15 M HNO_3 and 27 M HF, followed by equilibration in 6 M HCl was applied.

Supplementary Materials

This PDF file includes:

Supplementary Text
Figs. S1 to S29
Tables S1 to S7
References

REFERENCES AND NOTES

1. B. Frenzel, The Pleistocene vegetation of northern Eurasia. *Science* **161**, 637–649 (1968).
2. K. D. Bennett, P. C. Tzedakis, K. J. Willis, Quaternary refugia of North European trees. *J. Biogeogr.* **18**, 103–115 (1991).
3. G. H. Hewitt, The genetic legacy of the Quaternary ice ages. *Nature* **405**, 907–913 (2000).
4. D. T. Bilton, P. M. Mirol, S. Mascheretti, K. Fredga, J. Zima, J. B. Searle, Mediterranean Europe as an area of endemism for small mammals rather than a source for northwards postglacial colonization. *Proc. Biol. Sci.* **265**, 1219–1226 (1998).
5. R. J. Petit, I. Aguinagalde, J.-L. de Beaulieu, C. Bittkau, S. Brewer, R. Cheddadi, R. Ennos, S. Fineschi, D. Grivet, M. Lascoux, A. Mohanty, G. Müller-Starck, B. Demesure-Musch, A. Palmé, J. P. Martín, S. Rendell, G. G. Vendramin, Glacial refugia: Hotspots but not melting pots of genetic diversity. *Science* **300**, 1563–1565 (2003).
6. T. Schmitt, Z. Varga, Extra-Mediterranean refugia: The rule and not the exception? *Front. Zool.* **9**, 22 (2012).
7. C. M. Faria, P. Shaw, B. C. Emerson, Evidence for the Pleistocene persistence of Collembola in Great Britain. *J. Biogeogr.* **46**, 1479–1493 (2019).
8. K. J. Willis, T. H. Andel, Trees or no trees? The environments of central and eastern Europe during the Last Glaciation. *Quat. Sci. Rev.* **23**, 2369–2387 (2004).
9. L. Parducci, T. Jorgensen, M. M. Tollefsrud, E. Elverland, T. Alm, S. L. Fontana, K. D. Bennett, J. Haile, I. Matetovici, Y. Suyama, M. E. Edwards, K. Andersen, M. Rasmussen, S. Boessenkool, E. Coissac, C. Brochmann, P. Taberlet, M. Houmark-Nielsen, N. J. K. Larsen, L. Orlando, M. T. P. Gilbert, K. H. Kjaer, I. G. Alsos, E. Willerslev, Glacial survival of boreal trees in northern Scandinavia. *Science* **335**, 1083–1086 (2012).
10. J. R. Stewart, A. M. Lister, Cryptic northern refugia and the origins of the modern biota. *Trends Ecol. Evol.* **16**, 608–613 (2001).
11. P. Kotlík, V. Deffontaine, S. Mascheretti, J. B. Searle, A northern glacial refugium for bank voles (Clethrionomys glareolus). *Proc. Natl. Acad. Sci. U.S.A.* **103**, 14860–14864 (2006).
12. R. S. Sommer, A. Nadachowski, Glacial refugia of mammals in Europe: Evidence from fossil records. *Mammal Rev.* **36**, 251–265 (2006).
13. R. Vega, Phylogeographical structure of the pygmy shrew: Revisiting the roles of southern and northern refugia in Europe. *Biol. J. Linn. Soc.* **129**, 901–917 (2020).
14. H. J. B. Birks, K. J. Willis, Alpines, trees, and refugia in Europe. *Europe Plant Ecol. Div.* **1**, 147–160 (2008).
15. J. Provan, K. D. Bennett, Phylogeographic insights into cryptic glacial refugia. *Trends Ecol. Evol.* **23**, 564–571 (2008).
16. J. S. McLachlan, J. S. Clark, P. S. Manos, Molecular indicators of tree migration capacity under rapid climate change. *Ecology* **86**, 2088–2098 (2005).
17. R. Ohlemüller, B. Huntley, S. Normand, J. C, Svenning, Potential source and sink locations for climate-driven species range shifts in Europe since the Last Glacial Maximum. *Glob. Ecol. Biogeogr.* **21**, 152–163 (2012).
18. S. A. Leroy, K. Arpe, Glacial refugia for summer-green trees in Europe and south-west Asia as proposed by ECHAM3 time-slice atmospheric model simulations. *J. Biogeogr.* **34**, 2115–2128 (2007).
19. J.-C. Svenning, S. Normand, M. Kageyama, Glacial refugia of temperate trees in Europe: Insights from species distribution modelling. *J. Ecol.* **96**, 1117–1127 (2008).
20. K. Arpe, S. A. G. Leroy, U. Mikolajewicz, A comparison of climate simulations for the last glacial maximum with three different versions of the ECHAM model and implications for summer-green tree refugia. *Clim. Past* **7**, 91–114 (2011).
21. M. Slovák, J. Kučera, P. Turis, J. Zozomová-Lihová, Multiple glacial refugia and postglacial colonization routes inferred for a woodland geophyte, Cyclamen purpurascens: Patterns concordant with the Pleistocene history of broadleaved and coniferous tree species. *Biol. J. Linn. Soc.* **105**, 741–760 (2012).
22. J. Mitka, W. Bąba, K. Szczepanek, Putative forest glacial refugia in the Western and Eastern Carpathians. *Mod. Phytomorphol.* **5**, 85–92 (2014).
23. J. O. Kaplan, M. Pfeiffer, J. C. Kolen, B. A. Davis, Large scale anthropogenic reduction of forest cover in Last Glacial Maximum Europe. *PLOS ONE* **11**, 0166726 (2016).
24. P. C. Tzedakis, B. C. Emerson, G. M. Hewitt, Cryptic or mystic? Glacial tree refugia in northern Europe. *Trends Ecol. Evol.* **28**, 696–704 (2013).
25. J. A. Marshall, J. J. Roering, P. J. Bartlein, D. G. Granger, A. W. Rempel, S. J. Praskievicz, T. C. Hales, Frost for the trees: Did climate increase erosion in unglaciated landscapes during the late Pleistocene? *Sci. Adv.* **1**, 1500715 (2015).
26. M. Schaller, A 30 000 yr record of erosion rates from cosmogenic 10Be in Middle European river terraces. *Earth Planet. Sci. Lett.* **204**, 307–320 (2002).

27. J. Hošek, T. Radoměřský, M. Křížek, Late Glacial thermokarst phenomena on the northern margin of the Vienna Basin (Czech Republic). *Geosci. Res. Rep.* **53**, 65–72 (2020).
28. J. Kadlec, G. Kocurek, D. Mohrig, D. P. Shinde, M. K. Murari, V. Varma, F. Stehlik, V. Benes, A. K. Singhvi, Response of fluvial, aeolian, and lacustrine systems to late Pleistocene to Holocene climate change, Lower Moravian Basin, Czech Republic. *Geomorphology* **232**, 193–208 (2015).
29. R. O. Fournier, A. M. Pitt. The Yellowstone magmatichydrothermal system, USA. 1985 International Symposium on Geothermal Energy: International Volume. (Cal Central Press, Sacramento, 1985).
30. K. A. Campbell, Geyserite in hot–spring siliceous sinter: Window on Earth's hottest terrestrial (paleo)environment and its extreme life. *Earth Sci. Rev.* **148**, 44–64 (2015).
31. B. Y. Lynne, K. A. Campbell, J. N. Moore, P. R. L. Browne, Origin and evolution of the Steamboat Springs siliceous sinter deposit, Nevada, U.S.A. *Sediment. Geol.* **210**, 111–131 (2008).
32. B. Y. Lynne, Mapping vent to distal-apron hot spring paleo-flow pathways using siliceous sinter architecture. *Geothermics* **43**, 3–24 (2012).
33. J. B. Lowenstern, S. Hurwitz, J. P. McGeehin, Radiocarbon dating of silica sinter deposits in shallow drill cores from the Upper Geyser Basin, Yellowstone National Park. *J. Volcanol. Geotherm. Res.* **310**, 132–136 (2016).
34. S. Slagter, M. Reich, C. Munoz-Saez, J. Southon, D. Morata, F. Barra, J. Gong, J. R. Skok, Environmental controls on silica sinter formation revealed by radiocarbon dating. *Geology* **47**, 330–334 (2019).
35. S. Hurwitz, J. B. Lowenstern, Dynamics of the Yellowstone hydrothermal system. *Rev. Geophys.* **52**, 375–411 (2014).
36. A. P. G. Fowler, C. Tan, K. Luttrell, A. Tudor, P. Scheuermann, W. C. P. Shanks, W. E. Seyfried, Geochemical heterogeneity of sublacustrine hydrothermal vents in Yellowstone Lake, Wyoming. *J. Volcanol. Geotherm. Res.* **386**, 106677 (2019).
37. W. F. Fagan, A. Swain, A. Banerjee, H. Ranade, P. Thompson, P. P. A. Staniczenko, Quantifying interdependencies in geyser eruptions at the Upper Geyser Basin, Yellowstone National Park. *J. Geophys. Res. Solid Earth* **127**, e2021JB023749 (2022).
38. W. K. Buechler, Variability of venation patterns in extant genus *Salix*: Implications for fossil taxonomy. *PaleoBios.* **30**, 89–104 (2014).
39. A. Pereira, V. Ferreira, Invasion of native riparian forests by Acacia species affects in-stream litter decomposition and associated microbial decomposers. *Microb. Ecol.* **81**, 14–25 (2020).
40. R. Govaerts, D. G. Frodin, *World Checklist and Bibliography of Fagales* (Royal Botanic Gardens, 1998).
41. G. Lang, B. Ammann, K.-E. Behre, W. Tinner, *Quaternary Vegetation Dynamics of Europe* (Haupt Verlag, 2023).
42. J. H. Ietswaart, A. E. Feij, A multivariate analysis of introgression between *Quercus robur* and *Q. petraea* in The Netherlands. *Acta Bot. Neerl.* **38**, 313–325 (1989).
43. J. L. Dupouey, V. Badeau, Morphological variability of oaks (Quercus robur L, Quercus petraea (Matt) Liebl, Quercus pubescens Willd) in northeastern France: Preliminary results. *Ann. For. Sci.* **50**, 35s–40s (1993).
44. R. Bacilieri, A. Ducousso, A. Kremer, Genetic, morphological, ecological and phenological differentiation between *Quercus petraea* (Matt.) Liebl. and *Quercus robur L* in a mixed stand of Northwest of France. *Silvae Genetica* **44**, 1 (1995).
45. A. Kremer, J. L. Dupouey, J. D. Deans, J. Cottrell, U. Csaikl, R. Finkeldey, S. Espinel, J. Jensen, J. Kleinschmit, B. Van Dam, A. Ducousso, I. Forrest, U. L. de Heredia, A. J. Lowe, M. Tutkova, R. C. Munro, S. Steinhoff, V. Badeau, Leaf morphological differentiation between *Quercus robur* and *Quercus petraea* is stable across western European mixed oak stands. *Ann. For. Sci.* **59**, 777–787 (2002).
46. E. Barrón, A. Averyanova, Z. Kvaček, A. Momohara, K. B. Pigg, S. Popova, J. M. Postigo-Mijarra, B. Tiffney, T. Utescher, Z.-K. Zhou, *The Fossil History of Quercus* (Springer, 2017).
47. M. Hoffmann, U. Raeder, Predicting the potential distribution of neophytes in Southern Germany using native Najas marina as invasion risk indicator. *Environ. Earth Sci.* **75**, 1217 (2016).
48. B. Y. Lynne, K. A. Campbell, B. J. James, P. R. Browne, J. Moore, Tracking crystallinity in siliceous hot-spring deposits. *Am. J. Sci.* **307**, 612–641 (2007).
49. T. Howald, M. Person, A. Campbell, V. Lueth, A. Hofstra, D. Sweetkind, C. W. Gable, A. Banerjee, E. Luijendijk, L. Crossey, K. Karlstrom, S. Kelley, F. M. Phillips, Evidence for long timescale ($>10^3$ years) changes in hydrothermal activity induced by seismic events. *Geofluids* **15**, 252–268 (2015).
50. B. D. Drake, K. A. Campbell, J. V. Rowland, D. M. Guido, P. R. L. Browne, A. Rae, Evolution of a dynamic paleo-hydrothermal system at Mangatete, Taupo Volcanic Zone, New Zealand. *J. Volcanol. Geotherm. Res.* **282**, 19–35 (2014).
51. M. F. Soto, M. P. Hochstein, K. Campbell, H. Keys, Sporadic and waning hot spring activity in the Tokaanu Domain, Hipaua-Waihi-Tokaanu geothermal field, Taupo Volcanic Zone, New Zealand. *Geothermics* **77**, 288–303 (2019).
52. C. C. Munoz-Saez, M. Manga, S. Hurwitz, S. Slagter, D. Churchill, M. Reich, D. Damby, D. Morata, Radiocarbon dating of silica sinter and postglacial hydrothermal activity in the El Tatio geyser field. *Geophys. Res. Lett.* **47**, e2020GL087908 (2020).
53. D. M. Churchill, M. Manga, S. Hurwitz, S. Peek, J. Licciardi, J. B. Paces, Dating silica sinter (geyserite): A cautionary tale. *J. Volcanol. Geotherm. Res.* **402**, 106991 (2020).
54. C. M. Schiller, C. Whitlock, K. L. Elder, N. A. Iverson, M. B. Abbott, Erroneously old radiocarbon ages from terrestrial pollen concentrates in Yellowstone Lake, Wyoming, USA. *Radiocarbon* **63**, 321–342 (2021).
55. L. Steinke, G. W. Slysz, M. S. Lipton, C. Klatt, J. J. Moran, M. F. Romine, J. M. Wood, G. Anderson, D. A. Bryant, D. M. Ward, Short-term stable isotope probing of proteins reveals taxa incorporating inorganic carbon in a hot spring microbial mat. *Appl. Environ. Microbiol.* **86**, e01829-19 (2020).
56. A. Pasquier-Cardin, P. Allard, T. Ferreira, C. Hatte, R. Coutinho, M. Fontugne, M. Jaudon, Magma-derived CO_2 emissions recorded in ^{14}C and ^{13}C content of plants growing in Furnas caldera, Azores. *J. Volcanol. Geotherm. Res.* **92**, 195–207 (1999).
57. R. N. Holdaway, B. Duffy, B. Kennedy, Evidence for magmatic carbon bias in ^{14}C dating of the Taupo and other major eruptions. *Nat. Commun.* **9**, 4110 (2018).
58. S. Björck, B. Wohlfarth, *^{14}C Chronostratigraphic Techniques in Paleolimnology* (Kluwer Academic, 2001).
59. W. Finsinger, C. Schwörer, O. Heiri, C. Morales-Molino, A. Ribolini, T. Giesecke, J. N. Haas, P. Kaltenrieder, E. K. Magyari, C. Ravazzi, J. M. Rubiales, W. Tinner, Fire on ice and frozen trees? Inappropriate radiocarbon dating leads to unrealistic reconstructions. *New Phytol.* **222**, 657–662 (2019).
60. J. Holuša, D. Nývlt, B. Woronko, M. Matějka, R. Stuchlík, Environmental factors controlling the Last Glacial multi-phase development of the Moravian Sahara dune field, Lower Moravian Basin, Central Europe. *Geomorphology* **413**, 108355 (2022).
61. A. M. Seltzer, J. Ng, W. Aeschbach, Widespread six degrees Celsius cooling on land during the Last Glacial Maximum. *Nature* **593**, 228–232 (2021).
62. J. D. Annan, J. C. Hargreaves, A new global reconstruction of temperature changes at the Last Glacial Maximum. *Clim. Past* **9**, 367–376 (2013).
63. J. A. Nava, P. Morrison, A note on hot springs in the interior of Alaska. *Arctic* **27**, 241–243 (1974).
64. P. U. Clark, A. S. Dyke, J. D. Shakun, A. E. Carlson, J. Clark, B. Wohlfarth, J. X. Mitrovica, S. W. Hostetler, A. M. McCabe, The last glacial maximum. *Science* **325**, 710–714 (2009).
65. C. L. Parker, "Vascular plant inventory of Alaska'S Arctic National Parklands" (Tech. Rep. NPS/AKRARCN/NRTR-2006/01, National Park Service, 2006).
66. C. I. Fraser, A. Terauds, J. Smellie, P. Convey, S. L. Chown, Geothermal activity helps life survive glacial cycles. *Proc. Natl. Acad. Sci. U.S.A.* **111**, 5634–5639 (2014).
67. L. Strecker, "Botanical survey at Reed River Hot Springs, Gates of the Arctic National Park and Preserve (GAAR)" (Natural Resource Report NPS/GAAR/NRR-2016/1136, National Park Service, 2016).
68. Y. Kolosova, G. Potapov, N. Skyutte, I. Bolotov, Bumblebees (Hymenoptera, Apidae, Bombus Latr.) of the thermal spring Pymvashor, north-east of European Russia. *Entomologica Fennica.* **27**, 190–196 (2016).
69. E. Rybníčková, K. Rybníček, Palaeovegetation in the Pavlovské vrchy hills region (South Moravia, Czech Republic) around 25,000 BP: The Bulhary core. *Veg. Hist. Archaeobotany* **23**, 719–728 (2014).
70. E. Opravil, The vegetation, in *Pavlov I: Excavations 1952-1953* (*ERAUL 66/Dolní Věstonice Studies 2*), J. Svoboda, Ed. (Université de Liege, 1994), pp. 175–189.
71. F. Damblon, P. Haesaerts, J. Van der Plicht, New datings and considerations on the chronology of Upper Palaeolithic sites in the Great Eurasiatic Plain. *Préhistoire Européenne.* **9**, 177–231 (1996).
72. J. Novák, J. Roleček, P. Dresler, M. Hájek, Soil charcoal elucidates the role of humans in the development of landscape of extreme biodiversity. *Land Degrad. Dev.* **30**, 1607–1619 (2019).
73. A. Kröll, G. Wessely, R. Jiříček, F. Nemec, "Wiener Becken und angrenzende Gebiete-Geologische Einheiten des präneogenen Beckenuntergrundes" (Geologische Bundesanstalt, 1993).
74. E. Y. Lee, M. Wagreich, Polyphase tectonic subsidence evolution of the Vienna Basin inferred from quantitative subsidence analysis of the northern and central parts. *Int. J. Earth Sci.* **106**, 687–705 (2017).
75. K. Decker, H. Peresson, R. Hinsch, Active tectonics and Quaternary basin formation along the Vienna Basin Transform fault. *Quat. Sci. Rev.* **24**, 305–320 (2005).
76. M. W. Schmidt, J. E. Hertzberg, Abrupt climate change during the last ice age. *Nat. Educ. Knowledge* **3**, 11 (2011).
77. F. Fuhrmann, B. Diensberg, X. Gong, G. Lohmann, F. Sirocko, Aridity synthesis for eight selected key regions of the global climate system during the last 60 000 years. *Clim. Past* **16**, 2221–2238 (2020).
78. C. Prud'homme, Millennial-timescale quantitative estimates of climate dynamics in central Europe from earthworm calcite granules in loess deposits. *Commun. Earth Environ.* **3**, 267 (2022).
79. J. Vandenberghe, The Last Permafrost Maximum (LPM) map of the Northern Hemisphere: Permafrost extent and mean annual air temperatures, 25–17 ka BP. *Boreas* **43**, 652–666 (2014).

80. R. Martinez-Lamas, Linking Danube River activity to Alpine Ice-Sheet fluctuations during the last glacial (ca. 33–17 ka BP): Insights into the continental signature of Heinrich Stadials. *Quat. Sci. Rev.* **229**, 106136 (2020).
81. D. Pivko, R. Vojtko, A review of travertines and tufas in Slovakia: Geomorphology, environments, tectonic pattern, and age distribution. *Acta Geol. Slovaca* **13**, 49–78 (2021).
82. J. Seguinot, Modelling last glacial cycle ice dynamics in the Alps. *Cryosphere.* **12**, 3265–3285 (2018).
83. A. Sutkowska, A. K. Pasierbiński, T. Warzecha, A. Mandal, J. Mitka, Refugial pattern of Bromus erectus in Central Europe based on ISSR fingerprinting. *Acta Biol. Cracov. Bot.* **55**, 107–119 (2013).
84. K. J. Willis, P. Sümegi, M. Braun, A. Tóth, The late Quaternary environmental history of Bátorliget, N.E. Hungary. *Palaegeogr. Palaeoclimatol. Palaeoecol.* **118**, 25–47 (1995).
85. D. Magri, Patterns of post-glacial spread and the extent of glacial refugia of European beech (*Fagus sylvatica*). *J. Biogeogr.* **35**, 450–463 (2008).
86. L. Juřičková, J. Horáčková, V. Ložek, Direct evidence of central European forest refugia during the last glacial period based on mollusc fossils. *Quatern. Res.* **82**, 222–228 (2014).
87. A. Šolcová, Abrupt vegetation and environmental change since the MIS 2: A unique paleorecord from Slovakia (Central Europe). *Quat. Sci. Rev.* **230**, 106170 (2020).
88. Á. P. Molnár, L. Demeter, M. Biró, M. Chytrý, S. Bartha, B. Gantuya, Z. Molnár, Is there a massive glacial–Holocene flora continuity in Central Europe? *Biol. Rev.* **98**, 2307–2319 (2023).
89. K. Náfrádi, P. Sümegi, The Forest Refugium of the Bükk Mountains, Hungary—Vegetation Change and Human Impact from the Late Pleistocene. *Diversity* **16**, 109 (2024).
90. P. J. Reimer, The IntCal20 Northern Hemisphere radiocarbon age calibration curve (0–55 cal. kBP). *Radiocarbon* **62**, 725–757 (2020).
91. A. K. Raymer, T. Gobakken, B. Solberg, H. F. Hoen, E. Bergseng, A forest optimisation model including carbon flows: Application to a forest in Norway. *For. Ecol. Manage.* **258**, 579–589 (2009).
92. F. H. Schweingruber, *Microscopic Wood Anatomy: Structural Variability of Stems and Twigs in Recent and Subfossil Woods From Central Europe* (Zürcher, 1978).
93. W. Schoch, I. Heller, F. H. Schweingruber, F. Kienast, *Wood Anatomy of Central European Species* (Swiss Federal Institute for Forest, 2004).
94. B. E. Berglund, M. Ralska-Jasieviczowa, *Handbook of the Holocene Palaeoecology and Palaeohydrology* (Blackburn Press, 2003).
95. R. Martin, D. C. Mildenhall, P. R. Browne, K. A. Rodgers, The age and significance of in-situ sinter at the Te Kopia thermal area, Taupo Volcanic Zone New Zealand. *Geothermics* **29**, 367–375 (2000).
96. M. Reille, *Pollen et spores d'Europe et d'Afrique du Nord* (Laboratoire de Botanique historique et Palynologie, 1992).
97. M. Reille, *Pollen et spores d'Europe et d'Afrique du Nord - Supplement 1* (Laboratoire de Botanique historique et Palynologie, 1995).
98. M. Reille, *Pollen et spores d'Europe et d'Afrique du Nord - Supplement 2* (Laboratoire de Botanique historique et Palynologie, 1998).
99. H. J. Beug, *Leitfaden der Pollenbestimmung für Mitteleuropa und angrenzende Gebiete* (Verlag Dr. Friedrich Pfeil, 2004).
100. Z. D. Sharp, A laser-based microanalytical method for the in situ determination of oxygen isotope ratios of silicates and oxides. *Geochim. Cosmochim. Acta.* **54**, 1353–1357 (1990).
101. A. Pack, The oxygen isotope composition of San Carlos olivine on the VSMOW2-SLAP2 scale. *Rapid Commun. Mass Spectrom.* **30**, 1495–1504 (2016).
102. S. T. M. Peters, Triple oxygen isotope variations in magnetite from iron-oxide deposits, central Iran, record magmatic fluid interaction with evaporite and carbonate host rocks. *Geology* **48**, 211–215 (2020).
103. Z. D. Sharp, A calibration of the triple oxygen isotope fractionation in the SiO_2-H_2O system and applications to natural samples. *Geochim. Cosmochim. Acta.* **186**, 105–119 (2016).
104. J. A. G. Wostbrock, E. J. Cano, Z. S. D, An internally consistent triple oxygen isotope calibration of standards for silicates, carbonates and air relative to VSMOW2 and SLAP2. *Chem. Geol.* **533**, 119432 (2020).
105. A. Pack, Isotopic traces of atmospheric O2 in rocks, minerals, and melts. *Rev. Mineral. Geochem.* **86**, 217–240 (2021).
106. J. Ehlers, P. L. Gibbard, P. D. Hughes, *Quaternary Glaciations – Extent and Chronology* (Elsevier, 2011).
107. G. Wessely, Structure and development of the Vienna basin in Austria, in *The Pannonian Basin: A Study in Basin Evolution* (American Association of Petroleum Geologists, 1988), vol. 45, pp. 333–346.
108. T. Boldizsár, Geothermal data from the Vienna Basin. *J. Geophys. Res.* **73**, 613–618 (1968).
109. D. Husen, J. M. Reitner, An outline of the Quaternary stratigraphy of Austria. *Quat. Sci. J.* **60**, 366–387 (2011).
110. A. D. Miall, Architectural-element analysis: A new method of facies analysis applied to fluvial deposits. *Earth Sci. Rev.* **22**, 261–308 (1985).
111. P. J. Heaney, A proposed mechanism for the growth of chalcedony. *Contrib. Mineral. Petrol.* **115**, 66–74 (1993).
112. S. H. Butz, Silicification. *Paleontol. Soc. Paper* **20**, 15–34 (2014).
113. G. E. Mustoe, Wood petrifaction: A new view of permineralization and replacement. *Geosciences.* **7**, 119 (2017).
114. N. R. Herdianita, P. R. L. Browne, K. A. Rodgers, K. A. Campbell, Mineralogical and textural changes accompanying ageing of silica sinter. *Miner. Deposita* **35**, 48–62 (2000).
115. B. Y. Lynne, K. A. Campbell, J. Moore, P. R. L. Browne, Diagenesis of 1900-year-old siliceous sinter (opal-A to quartz) at Opal Mound, Roosevelt Hot Springs, Utah, U.S.A. *Sediment. Geol.* **119**, 249–278 (2005).
116. J. Surma, S. Assonov, M. Staubwasser, Triple oxygen isotope systematics in the hydrologic cycle. *Rev. Mineral. Geochem.* **86**, 401–428 (2021).
117. A. Pack, D. Herwartz, The triple oxygen isotope composition of the Earth mantle and understanding ΔO^{17} variations in terrestrial rocks and minerals. *Earth Planet. Sci. Lett.* **390**, 138–145 (2014).
118. S. Geilert, Silicon isotope fractionation during precipitation from hot-spring waters: Evidence from the Geysir geothermal field, Iceland. *Geochim. Cosmochim. Acta.* **164**, 403–427 (2015).
119. D. T. Wilmeth, Depositional evolution of an extinct sinter mound from source to outflow, El Tatio, Chile. *Sediment. Geol.* **406**, 105726 (2020).
120. J. L. Feng, Z. H. Zhao, F. Chen, H. P. Hu, Rare earth elements in sinters from the geothermal waters (hot springs) on the Tibetan Plateau, China. *J. Volcanol. Geotherm. Res.* **287**, 1–11 (2014).
121. E. Anders, N. Grevesse, Abundances of the elements: Meteoritic and solar. *Geochim. Cosmochim. Acta* **53**, 197–214 (1989).
122. R. L. Rudnick, S. Gao, Composition of the continental crust, in *The Crust Treatise on Geochemistry*, H. D. Holland, K. K. Turekian, Eds. (Elsevier, 2003), vol. 4, pp. 1–64.
123. A. Hamilton, K. Campbell, D. M. Guido, *Atlas of Siliceous Hot Spring Deposits (Sinter) and Other Silicified Surface Manifestations in Epithermal Environments* (Institute of Geological and Nuclear Sciences Limited, 2019).
124. A. Remšík, "Liptov Basin—Regional hydrogeothermal evaluation" (Final report, Ministry of Environment, 1998).
125. H. A. Waldrop, K. L. Pierce, "Surficial geologic map of the Madison Junction quadrangle, Yellowstone National Park, Wyoming" (Miscellaneous Investigations I-651, US Geological Survey, 1975).
126. T. R. Schneider, W. D. McFarland, "Hydrologic data and description of a hydrologic monitoring plan for the Borax Lake area" (Open-File Report 95-367, US Geological Survey, 1995); https://doi.org/10.3133/ofr95367.

Acknowledgments: We are grateful to J. Roleček and F. Lysák for drawing our attention to the circular structures. We thank C. Campbell (University of Auckland, New Zealand) and D. Guido (Instituto de Recursos Minerales, Argentina) for help and fruitful discussions during the fieldwork in YNP. O. Sobek is acknowledged for help with the visualization of leaf venation patterns and E. Antalová and O. Šebek for the determination of major element compositions. The fieldwork in YNP was conducted under research permits YELL-2022-SCI-7020. **Funding:** The research was supported by the Czech Scientific Foundation (projects numbers 21-23196S, 23-05132S, and 23-07625S), the Czech Ministry of Culture (IP DKRVO 2024-2028 2.II.a, National Museum, 00023272), Charles University Research Centre program no. UNCE/24/SCI/006, Operational Programme of the Ministry of Education Youth and Sports of the Czech Republic under the project "RAMSES" (CZ.02.1.01/0.0/0.0/16_019/0000728), and long-term research development project of the Institute of Botany of the Czech Academy of Sciences (RVO 67985939). The fieldwork of J.Ho. in YNP was supported by the Researcher Mobility Program no. CZ.02.2.69/0.0/0.0/18_053/0017379-1). This is a contribution to the Strategic Research Plan of the Czech Geological Survey (DKRVO/ČGS 2023-2027). **Author contributions:** J.Ho. and P.P. conceptualized the project; J.Ho. was responsible for its management and undertook the fieldwork along with T.R., M.K., P.P., P.H., E.J., and J.N. Pollen analyses were performed by P.P. and E.J.; plant macro-remains were analyzed by J.K., J.N., and P.H. T.M., F.L., V.R., A.P., and T.D.R. arranged the geochemical analyses. L.B., J.Ha., and J.Ho. performed petrographic investigations. J.Ha., T.H., L.B., and J.Ho. designated the fieldwork and sampling in the Yellowstone National Park. Data visualization was undertaken by J.Ho. The original manuscript was drafted by J.Ho., P.P., I.H., and D.S. Editing of the manuscript was undertaken by J.Ho., I.H., D.S., and P.P. with contributions from all authors. **Competing interests:** The authors declare that they have no competing or conflicting interests. **Data and materials availability:** All data needed to evaluate the conclusions in the paper are present in the paper and/or the Supplementary Materials. Study material is available in the repositories of the Czech Geological Survey and National Museum, Prague.

Submitted 18 February 2024
Accepted 30 April 2024
Published 31 May 2024
10.1126/sciadv.ado6611